Clim Dyn (2009) 32:355–369
DOI 10.1007/s00382-008-0386-6

Evaluation of tropical cloud regimes in observations and a general circulation model

Yonghua Chen · Anthony D. Del Genio

Received: 30 August 2007 / Accepted: 19 February 2008 / Published online: 6 March 2008

Abstract Tropical cloud regimes defined by cluster analysis of International Satellite Cloud Climatology Project (ISCCP) cloud top pressure (CTP)–optical thickness distributions and ISCCP-like Goddard Institute for Space Studies (GISS) general circulation model (GCM) output are analyzed in this study. The observations are evaluated against radar–lidar cloud-top profiles from the atmospheric radiation measurement (ARM) Program active remote sensing of cloud layers (ARSCL) product at two tropical locations and by placing them in the dynamical context of the Madden–Julian oscillation (MJO). ARSCL highest cloud-top profiles indicate that differences among some of the six ISCCP regimes may not be as prominent as suggested by ISCCP at the ARM tropical sites. An experimental adjustment of the ISCCP CTPs to produce cloud-top height profiles consistent with ARSCL eliminates the independence between those regimes. Despite these ambiguities, the ISCCP regime evolution over different phases of the MJO is consistent with existing MJO mechanisms, but with a greater mix of cloud types in each phase than is usually envisioned. The GISS Model E GCM produces two disturbed and two suppressed regimes when vertical convective condensate transport is included in the model's cumulus parameterization. The primary model deficiencies are the absence of an isolated cirrus regime, a lack of mid-level cloud relative to ARSCL, and a tendency for occurrences of specific parameterized processes such as deep and shallow convection and stratiform low cloud formation to not be associated preferentially with any single cloud regime.

Keywords Cluster analysis · Tropical cloud regimes · GISS Model E · ARSCL · ISCCP D1 · MJO

Y. Chen (✉)
Department of Applied Physics and Applied Mathematics, Columbia University and Institute for Space Studies, 2880 Broadway, New York, NY 10025, USA
e-mail: ychen@giss.nasa.gov

A. D. Del Genio
NASA Goddard Institute for Space Studies, New York, NY, USA

1 Introduction

Errors in cloud feedback estimation in general circulation models (GCMs) are associated with both incorrect occurrences of different cloud regimes and errors in the cloud properties within these regimes. Evaluations of clouds in the GCMs have been done recently using the concept of regimes that are either dynamically based (e.g. Bony et al. 2004; Norris and Weaver 2001) or cloud property based (e.g. Williams et al. 2005; Gordon et al. 2005). It is important, however, to understand the limitations of observations before evaluating GCMs using them.

The k-means clustering method was first applied to 1 year of International Satellite Cloud Climatology Program (ISCCP) D1 joint histograms of cloud top pressure (CTP) and optical thickness by Jakob and Tselioudis (2003, hereafter JT03) to identify 4–5 major cloud regimes in the Tropical Western Pacific region (TWP). Jakob et al. (2005) further discussed the cloud, radiative and thermodynamic properties within those cloud regimes based on 2 years of data. Rossow et al. (2005) extended the study to the whole tropics within ±15°N latitude using 21.5 years of data, and identified six distinct so-called weather states. Recent results from CloudSat data show some consistency with this classification of six weather states (Zhang et al. 2007). With the development of the ISCCP simulator (Klein and Jakob 1999;

Webb et al. 2001), this clustering approach has been further applied to GCM output and as a tool to evaluate the performance of GCM cloud parameterizations (e.g. Gordon et al. 2005; Williams and Tselioudis 2007, hereafter WT07).

Drawing conclusions from such model-data comparisons is not straightforward, however. For example, Zhang et al. (2005) show that GCMs uniformly underpredict mid-level top clouds relative to ISCCP. However, passive remote sensing approaches are known to incorrectly locate cloud top in the presence of errors in the input temperature and moisture profiles and in multilayer cloud situations (Wang al. 1999; Chang and Li 2005; Del Genio et al. 2005). Considering that the ISCCP histograms are now being used to make inferences about climate sensitivity (Murphy et al. 2004; WT07), it is necessary to understand the impact of the limitations of ISCCP on the cloud regimes derived from it. Second, the weather states are inferred from cloud properties but tend to be associated with specific dynamic phenomena. Before interpreting model-data discrepancies in terms of any particular physical process (e.g. convection), it would be useful to see how well these processes actually correspond to the cloud regimes that are supposed to represent them.

To achieve this, we attempt in this paper to put the observed tropical cloud regimes into perspective in two ways. First, we evaluate the ISCCP tropical cloud regime classification against active remote sensing cloud profiles at Tropical West Pacific (TWP) locations. Second, we evaluate the ability of the ISCCP cloud regime classification to capture well-documented dynamical variations of cloud structure associated with the Madden–Julian Oscillation (MJO; Madden and Julian 1971, 1994; Stephens et al. 2004; Lau and Waliser 2005; Zhang 2005; Benedict and Randall 2007). Then finally, we examine the performance of the Goddard Institute for Space Studies (GISS) GCM's simulation of cloud regimes, including physical processes associated with each regime, and discuss the possible reasons behind the differences between observed and modeled cloud regimes.

The paper is organized as follows. The observations, GISS GCM, and clustering method used to define the cloud regimes are described in Sect. 2. The results from the observational analyses are presented and discussed in Sect. 3 followed by those from the GISS GCM in Sect. 4. Section 5 summarizes our results and conclusions.

2 Data, model and methodology

2.1 Data sources

2.1.1 ISCCP D1 3-hourly CTP–TAU histograms

The ISCCP D1 product (Rossow and Schiffer 1999) gives joint histograms of CTP and cloud optical thickness (TAU) occurrence distributed in six TAU and seven CTP categories every 3 h within a 2.5°× 2.5° grid box. Its coverage is limited to sunlit points. Ideally, the CTP–TAU histogram gives a distribution of the highest cloud tops. In reality, limitations of the algorithm and input datasets introduce uncertainties in CTP in situations with optically thin or multiple-layer clouds present. The algorithm classifies thin clouds whose top cannot definitively be located as thin cirrus.

2.1.2 ARSCL cloud top and base measurements at the TWP sites

The active remote sensing of cloud layers (ARSCL) product (Clothiaux et al. 2000) provides cloud top and base measurements from millimeter cloud radar, micropulse lidar, and ceilometer instruments at the atmospheric radiation measurement (ARM) Program's TWP sites on Manus and Nauru Islands. ARSCL data provide a detailed cloud vertical distribution with a vertical resolution of 45 m, and temporal resolution of 10 s. In this paper, this data set is binned into 30-min intervals at the ISCCP vertical resolution, which then is used to calculate the distribution of highest cloud tops over a 3-h period coincident with ISCCP. To obtain the actual cloud fraction as a function of height during the same 3-h period, we separately bin the original dataset at 30-min temporal resolution and 250 m vertical intervals, then obtain the all-height cloud profiles.

Other ARM products at the TWP used in this study are surface precipitation and sounding profiles for relative humidity, pressure, temperature and altitude.

2.1.3 MJO index

An MJO index is used in this study to estimate the date (in pentads) that the peak of an MJO event passes different longitudes. The index is based on extended empirical orthogonal function analysis of 200 hPa velocity potential anomalies. It has ten components centered at 20°E, 70°E, 80°E, 100°E, 120°E, 140°E, 160°E, 120°W, 40°W and 10°W, respectively. Negative (positive) values represent enhanced (suppressed) convection. We consider a strong MJO event to be one with a negative index <-1. The index is available from the National Oceanic and Atmospheric Administration's Climate Prediction Center (http://www.cpc.noaa.gov/products/precip/CWlink/daily_mjo_index/pentad.html).

2.2 GISS global climate model description

We use the GISS Model E GCM described in Schmidt et al. (2006) but with an updated moist convection scheme including diagnosed updraft speeds and entrainment rates

(Del Genio et al. 2007) and vertical convective condensate transport. We run Model E at a horizontal and vertical resolution of 2°× 2.5°× 32 L. The simulation is forced by observed sea surface temperature and sea ice cover from the Hadley Center for Climate Prediction and Research (Rayner et al. 2003) for the period December 1998 to December 2003. Diagnostics for this study include 3-hourly ISCCP-like CTP–TAU histograms using the ISCCP simulator (version 3.5; Klein and Jakob 1999; Webb et al. 2001) with a mixed maximum-random overlap assumption, shallow and deep convection occurrence, and stratiform cloud occurrence and cover at each half-hour model physics time step.

The Model E cumulus parameterization uses an updraft mass flux closure that produces neutral buoyancy at cloud base. The mass flux is partitioned into two plumes that entrain at different rates based on buoyancy and updraft speed. Detrainment occurs at the level of neutral buoyancy. Convective motions transport momentum from their level of origin via a simple down-gradient momentum-mixing scheme. Convective cloud cover is classified as shallow if the top of the cloud is below the 700 mb level, which is within the two lowest intervals of the ISCCP CTP distribution, and as deep if the thickness of the cloud is larger than 450 mb.

In the model version used by Del Genio et al. (2007), convective condensate is partitioned into precipitating and detraining parts by dividing an assumed Marshall–Palmer drop size distribution into parts for which fallspeeds do or do not exceed the local updraft speed. For the run described in this paper, only particles with fallspeeds close enough to the updraft speed to remain in each layer detrain there; those with greater speeds precipitate as before, while those with smaller fallspeeds are advected up to the next model layer.

The stratiform cloud scheme diagnoses cloud fraction based on relative humidity and stability and divides the non-convective portion of a grid box into cloudy and clear parts with different relative humidities. Cloud water content is prognostic, including simple representations of all microphysical processes (autoconversion, accretion, Bergeron–Findeisen diffusional growth, evaporation, cloud-top entrainment). TAU is diagnosed from the cloud water path assuming different fixed particle number concentrations for continental liquid, ocean liquid, and ice clouds.

2.3 Cluster analysis method

A k-means clustering algorithm (cf. Anderberg 1973) is applied to 3-hourly ISCCP CTP–TAU histograms. In this study, a data unit refers to a 42-element vector in a CTP–TAU joint distribution histogram. The number of clusters, k, is specified at the beginning of the algorithm. The initial cluster centroids are chosen randomly from the data set. Iteratively, the algorithm optimizes the centroids by minimizing the sum of within-cluster distance to the centroids. At each step, the algorithm assigns each data unit to the cluster with the nearest centroid as measured by the Euclidean distance. A new set of centroids is generated at the end of each iteration. Since k-means cluster analysis is sensitive to initial seeds, especially if outliers exist, the process is repeated 40 times (100 times for the GCM, whose gridboxes contain less information than an instantaneous ISCCP histogram) to ensure a dominant set of cluster patterns.

In practice, we remove completely clear-sky data units before clustering because as suggested by WT07, this helps with the stability of the GCM clusters and has little effect on the ISCCP clusters. We analyze only 5 years of ISCCP data and GCM simulations (1999–2003) instead of the full 21.5 years of data analyzed by Rossow et al. (2005). WT07 have shown that this choice makes little impact on the results.

Empirical approaches to determine the final set of clusters were described in previous studies of clustering of ISCCP D1 histograms (e.g. JT03; Rossow et al. 2005; Gordon et al. 2005; WT07). We follow the process described by WT07 to judge the outcome, starting with the number of assumed clusters as 2, and then increasing the number until the criteria are no longer met. Specifically, the criteria include: the correlation between any two resulting cluster centroids must be less than 0.9; the least common cluster must have a relative frequency of occurrence (RFO) of at least 3.5%; the final set of clusters has to appear more than half the time in the repeated analysis. Some clusters with similar characteristics are subjectively combined at the end of the process to focus on a set of "principal cloud regimes" that can be directly compared with those of WT07.

3 Observed tropical cloud regimes

In this section, we show the results from cluster analysis on ISCCP 3-hourly CTP–TAU histograms from 1999 to 2003 over 15°N–15°S. This is the same latitude band analyzed by Rossow et al. (2005). Expansion of the study regions to higher latitudes (WT07) produces similar clusters except for the addition of a distinctly extratropical frontal cluster. After identifying the cloud regimes, we further examine the cloud vertical distribution for each cloud regime using ARSCL measurements. We then discuss how the cloud regimes evolve over different phases of the MJO.

3.1 Regimes from ISCCP D1 data

Analysis of ISCCP histograms yields a set of seven clusters in 68% of the 40 repetitions, with an additional

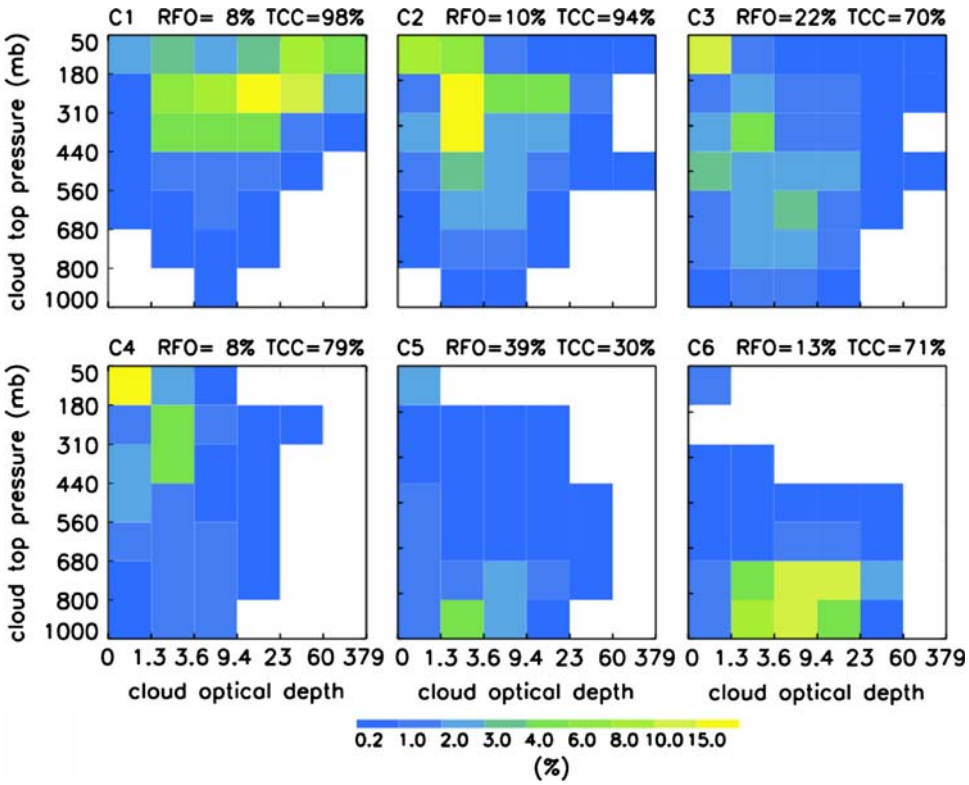

Fig. 1 Mean CTP–TAU histograms of six clusters from 3-hourly ISCCP D1 data over the tropical region of 15°N–15°S. Relative frequency of occurrence (*RFO*) and total cloud cover (*TCC*) are given for each cluster

stratocumulus cloud regime compared to that in Rossow et al. (2005). We combined these two stratocumulus regimes because of the similarity of their CTP–TAU histograms, cloud cover, and geographical distributions. Figure 1 shows the final set of six centroid histograms, with the corresponding geographic map of the frequency of occurrence for each cluster in Fig. 2. As in Rossow et al. (2005), clusters C1–C4 correspond to regimes dominated by deep convective clouds, cirrostratus anvils, mid-level cumulus congestus, and isolated cirrus, respectively, which all occur preferentially in the Intertropical Convergence Zone (ITCZ) and South Pacific Convergence Zone (SPCZ). The other two clusters represent suppressed cloud regimes: shallow trade cumulus over the central/east Pacific, and marine stratocumulus off the west coast of South America.

To check how representative these tropical regimes are of conditions at the TWP sites, the mean histogram for each cluster is constructed by averaging all available histograms at the grid box containing a given TWP site. The main features of the joint CTP–TAU distribution are retained at the TWP sites, but the RFOs differ (figure not shown). The first five regimes occur with roughly equal frequency at Manus while the stratocumulus regime is very infrequent, unlike the behavior of the tropics as a whole. At Nauru, the cirrus regime (cluster 4) occurs more often than for the tropics as a whole. The correlations between pairs of histograms of cloud regimes C2–C6 increase slightly at Manus and Nauru compared to those for the whole tropics, especially that between C3 and C4, which exceeds 0.9. This suggests that C3 and C4 are no longer independent regimes at the two TWP sites. This result is consistent with previous studies (JT03, Jakob et al. 2005) using ISCCP data only from the TWP region for cluster analysis, which found either four or five independent regimes.

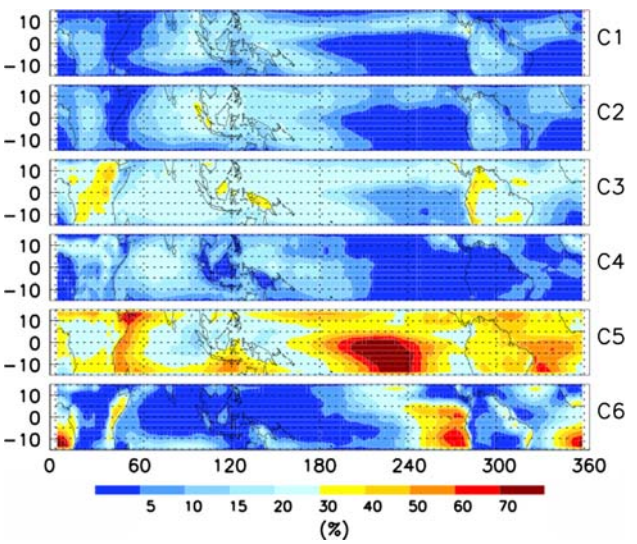

Fig. 2 The corresponding geographic distribution maps of the frequency of occurrence for each cluster in Fig. 1

3.2 Vertical cloud distribution of TWP cloud regimes

In this section, the cloud vertical structure for each cloud regime is examined at Manus and Nauru using ARSCL cloud profiles. For the grid box containing a TWP site, we obtain a time series of ISCCP cluster indices from the tropics-wide clusters. A 3-hourly ARSCL profile created from the 30-min binned cloud counts from lidar/radar instruments is assigned to the relavent ISCCP cluster. Then the mean ARSCL profile for a given regime is obtained by averaging within each cluster. First we examine the distribution of ARSCL highest cloud-tops only, which is the primary control on longwave cloud forcing and comparable to what ISCCP sees. Next, we extend the analysis to construct all-level cloud profiles like those in Jakob et al. (2005) and Gordon et al. (2005). Finally we divide the ISCCP histograms at Manus and Nauru into two subgroups: cases when ISCCP agrees with ARSCL (to within 10% in cloud fraction in every layer) and cases when they disagree. Then we examine the differences between those two subgroups in each cloud regime.

Figures 3 and 4 show the time mean vertical distribution of the highest cloud-top for each cloud regime at Manus and Nauru from ARSCL (solid lines) and ISCCP (dashed lines) data. ARSCL highest cloud-tops occur most often at 11–15 km in all regimes. ISCCP cloud-top profiles differ more between cloud regimes than do those for ARSCL. There is a much higher percentage of mid-level cloud-tops in less disturbed and more suppressed conditions (e.g. C3 and C4), while low cloud occurrence is underestimated, especially at Nauru. The percentage of high clouds in the cirrus regime (C4) is overestimated as well. For the trade cumulus and stratocumulus regimes (C5 and C6), ISCCP misses the high altitude peak.

A few factors may contribute to these discrepancies. One is the choice of comparing ARSCL profiles with ISCCP clusters obtained from tropics-wide clustering, This may partially explain the similarity between C3 and C4, which are not always separated clusters when ISCCP data over only the TWP are clustered (JT03, Jakob et al. 2005). Another is the additional TAU information in ISCCP data but missing from ARSCL. However, the discrepancies also partially arise from incorrect input temperature and humidity profiles, and from overlapping cirrus and low clouds that ISCCP cannot distinguish (Wang et al. 1999; Chang and Li 2005; Del Genio et al. 2005). The ISCCP mid-level cloud bias is of particular interest. For example, Zhang et al. (2005) conclude that all GCMs underestimate mid-level clouds based on ISCCP. Of greater concern, perturbed parameter ensemble simulations use agreement with ISCCP histograms as one metric for weighting climate sensitivity estimates (Murphy et al. 2004). WT07 also propose constraining the variation in climate sensitivity among models by evaluation of the present-day cloud

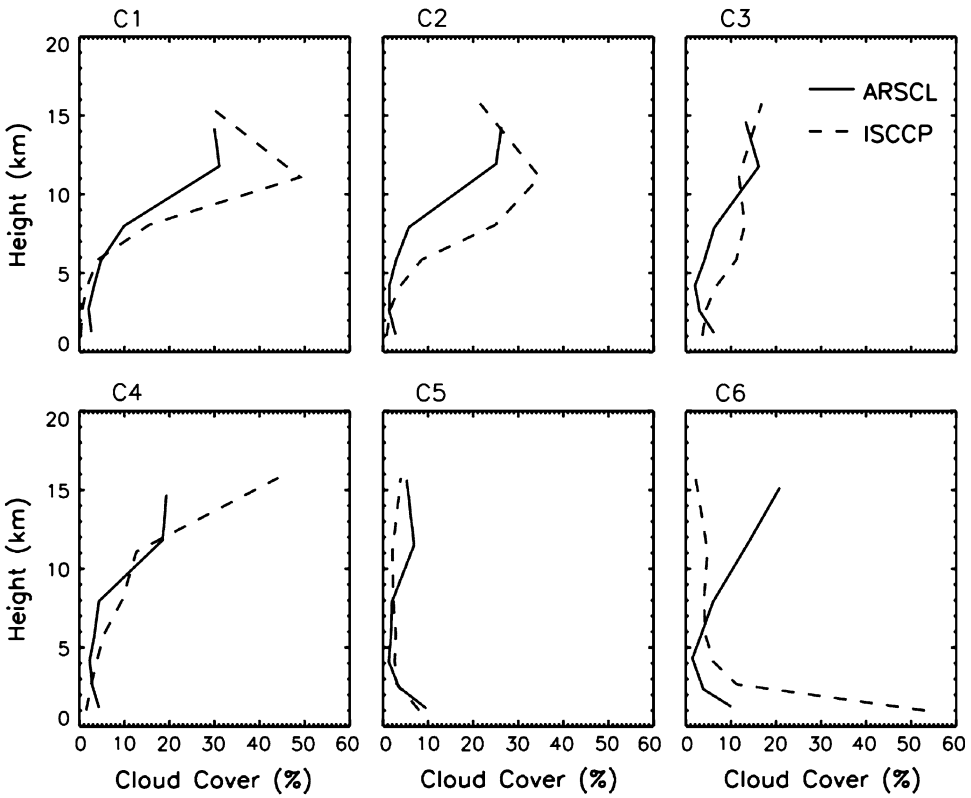

Fig. 3 Mean highest cloud-top vertical profiles from ARSCL (*solid*) and ISCCP CTP–TAU histograms (*dashed*) for each cloud regime at Manus. A mean sounding was used to convert ISCCP CTP to height

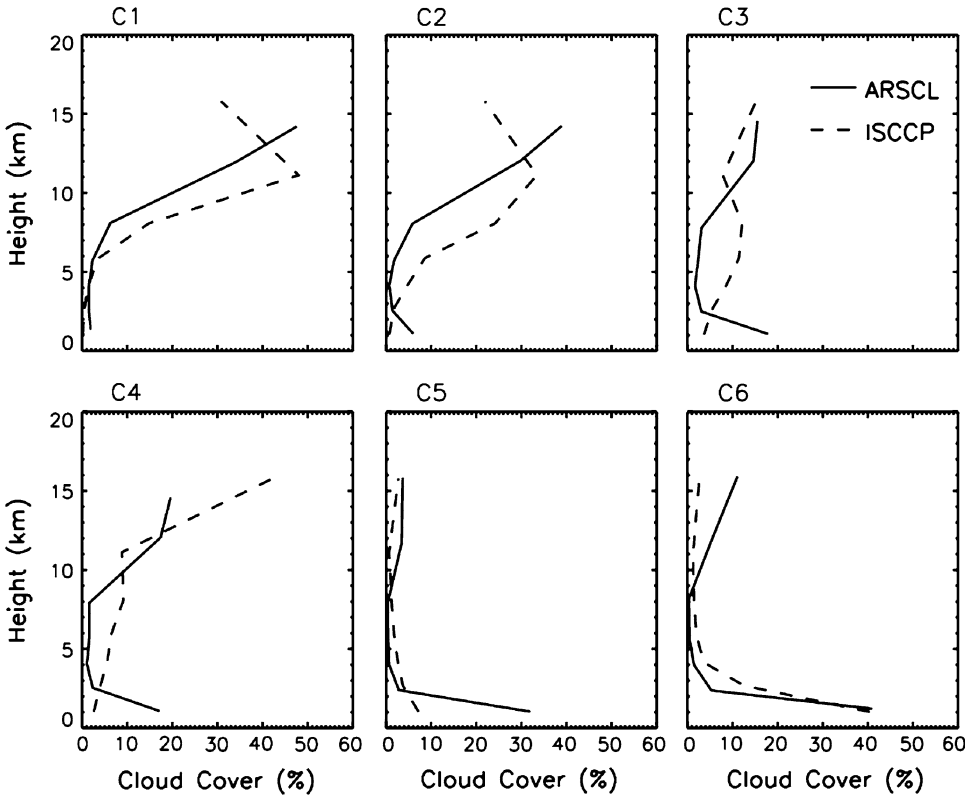

Fig. 4 As in Fig. 3 but at Nauru

regimes in GCMs against ISCCP. In principle the ISCCP simulator should handle these situations, but only limited tests have been performed (Del Genio et al. 2005). Finally, Figs. 3 and 4 raise the possibility that ISCCP cluster separation may be partly an artifact of its retrieval limitations, since the ARSCL profiles are so similar for each cloud regime.

To gain further insight into this question, we examine the all-level cloud profiles for each regime at Manus and Nauru (Fig. 5). The results agree well with those in Jakob et al. (2005, Fig. 4), which are based on only 17 months of data, with the exception that the peak in low-level cloud in the deep convection regime (C1) is more prominent here. The large amount of cloud cover below about 5 km is itself partly biased due to the ambiguity of the cloud radar retrieval when precipitation is occurring. As mentioned in Jakob et al. (2005), the low level cloud fraction seen by cloud radar increases when the cloud regime shifts to more convectively active states, while it decreases in passive satellite measurements (e.g. ISCCP) because of their inability to penetrate the optically thick clouds to detect low-level clouds. Notably, though, all regimes except shallow cumulus (C5) contain significant middle-level cloud, although these may be a mix of cumulus congestus and deeper clouds. The C3 and C4 profiles are quite similar, the latter having slightly more and higher high cloud.

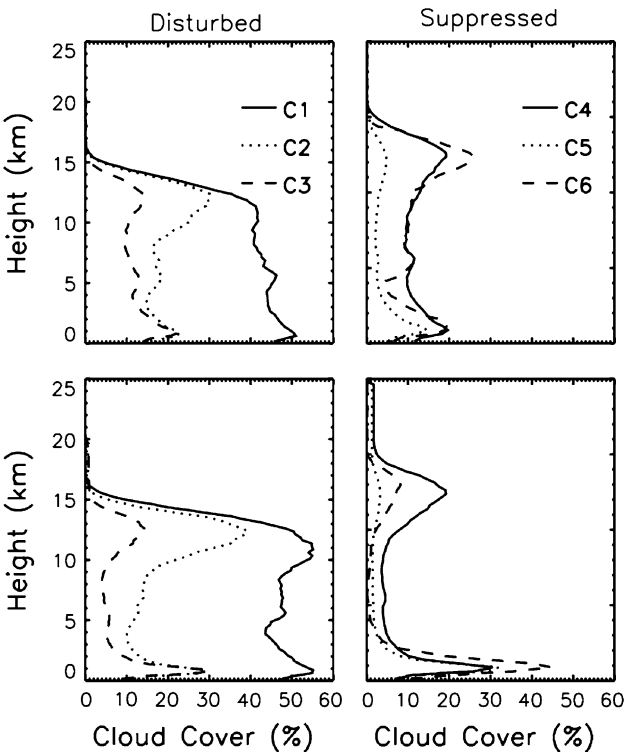

Fig. 5 Mean ARSCL cloud fraction profiles at 250 m resolution for each ISCCP cluster at Manus (*upper panels*) and Nauru (*lower panels*). The *left panels* represent the disturbed states (C1, C2, C3) and the *right panels* the suppressed states (C4, C5, C6)

Based on the differences between the instantaneous ARSCL and ISCCP cloud-top profiles used to create Figs. 3 and 4, we divide the histograms at Manus and Nauru into two groups: cases when ARSCL and ISCCP agree (i.e., differences at all levels are less than 10%), and cases when at least at one level they disagree by more than 10%. Only results for regimes C1–C4 are shown (Fig. 6) because the two datasets always disagree in the shallow cumulus regime while the stratocumulus regime occurs very infrequently.

In general ISCCP is most accurate when either convection penetrates often to the highest level (C1) or when cirrus are detected most often near the tropopause (C2, C4). Disagreements tend to occur when ISCCP detects more clouds of low to mid-range optical thickness (C1–C3), which may reflect biases due to partly cloud-covered pixels. The Euclidean distances between the clusters that agree versus disagree with ARSCL (Table 1) are greatest for the most disturbed states (11–18%); these can be considered crude retrieval error bars for our assessment of GCM cloud regimes in Sect. 4.

Figure 6 indicates that errors occur preferentially at different optical thicknesses for different cloud regimes. Bearing this limitation in mind, we create synthetic "corrected" ISCCP histograms by uniformly adjusting the CTP distributions in all TAU categories to be consistent with the ARSCL cloud-top profiles. The adjusted regime histograms for Manus (not shown) indicate that regimes C2, C3, and C4 are now quite similar to each other. The correlations exceed 0.9 between C4 and C2 and between C4 and C3 at Manus, and between C4 and C3 at Nauru. We also applied a similar correction based on the averaged differences at Manus and Nauru to the histograms for the entire tropics in Fig. 1 (not shown). Again C3 and C4 are no longer independent of each other with a correlation larger than 0.9. This indicates a potential uncertainty in the classification of C2, C3 and C4 as independent regimes. The high correlations suggest that subtle optical thickness differences (apparently smaller than the width of an ISCCP TAU bin) between these regimes are manifested primarily by their effect on the ISCCP retrieval of CTP.

Table 1 Euclidean distance (%) between the mean ISCCP CTP–TAU histograms for cases whose highest cloud-top heights agree with ARSCL and for those that disagree at Manus and Nauru for each cluster

TWP sites	Cluster					
	C1	C2	C3	C4	C5	C6
Manus	17.8	16.4	5.3	9.1	–	–
Nauru	13.2	10.9	8.9	8.9	–	7.5

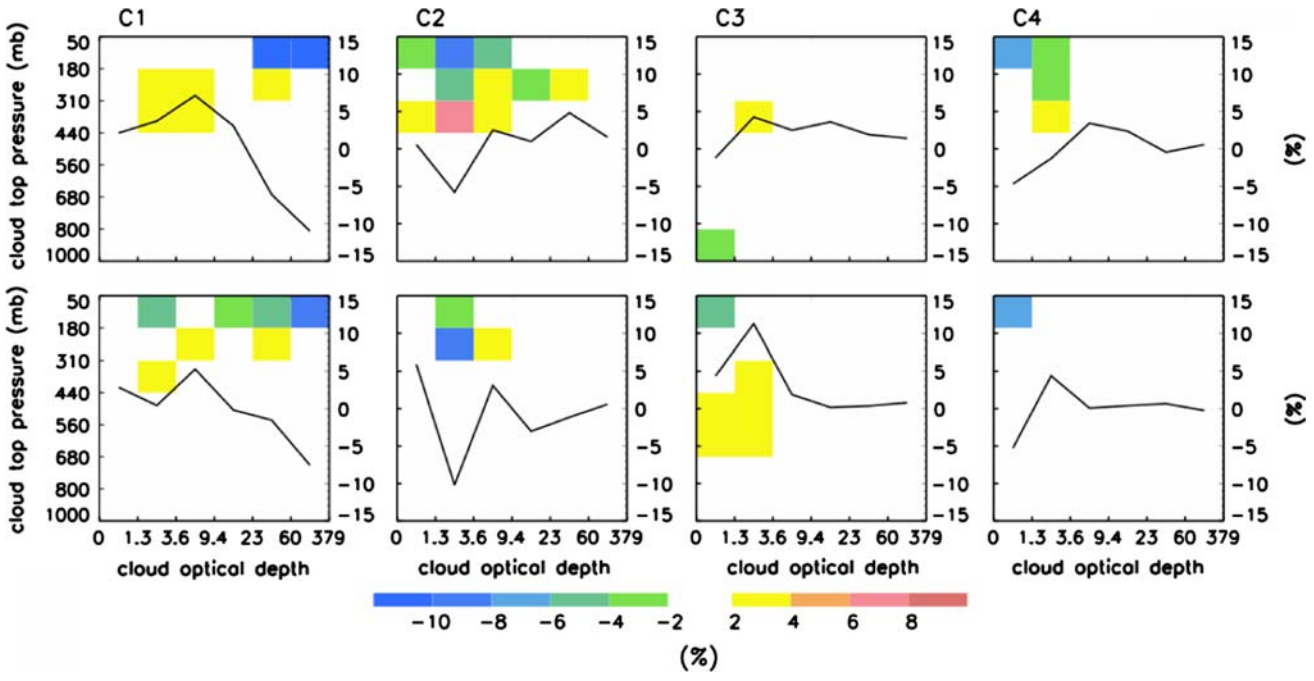

Fig. 6 Differences in CTP–TAU histograms for each cloud regime between cases when ISCCP and ARSCL disagree minus those for cases when they agree. The *solid line* is the vertically summed difference for each ISCCP TAU interval (scale given in percent on the right ordinate). *Upper panel* is for Manus, and *bottom* is for Nauru. Negative values mean that ISCCP underestimates the given cloud type

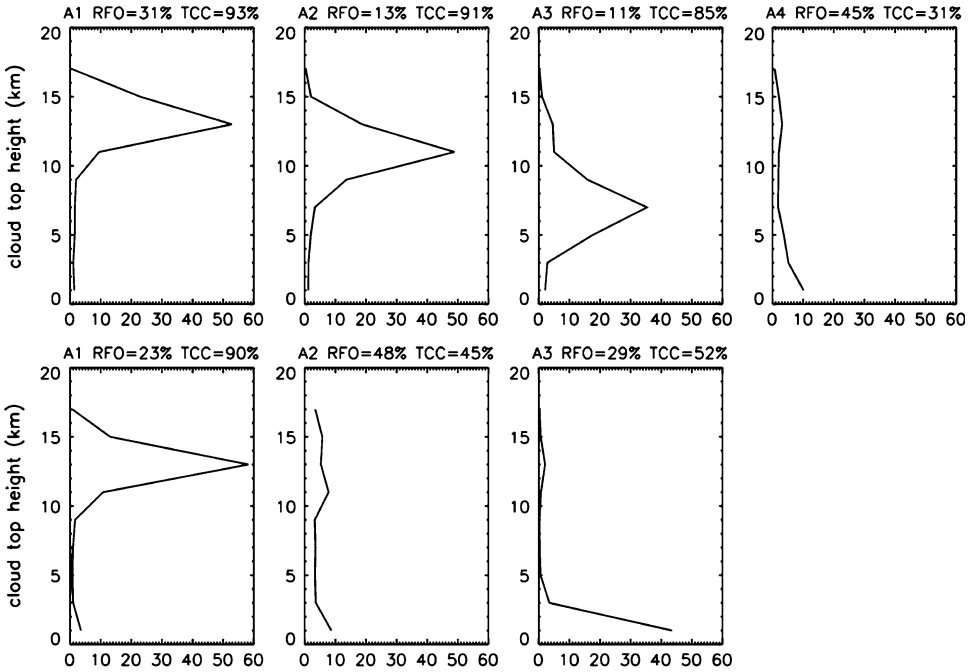

Fig. 7 Mean highest cloud-top profiles for ARSCL clusters at Manus (*top panel*) and Nauru (*lower panel*) based on all available 3-hourly ARSCL data

3.3 Regimes from ARSCL profiles

To further explore the independence of clusters, we apply the same clustering algorithm directly to the ARSCL cloud top height profiles. We first aggregate the ARSCL highest cloud-top profiles at 3-hourly temporal resolution and 2 km vertical resolution from 1999 to 2003 at Manus and Nauru. Then we cluster all available profiles, as well as daytime only profiles that match the times of ISCCP retrievals.

Figure 7 shows the ARSCL clusters at Manus (upper panel) and Nauru (lower panel). Four independent clusters are obtained at Manus, in $\sim$2/3 of the repetitions. The dominant cluster (A1) has a peak around 13 km, and the second most frequent cluster (A4) is a suppressed low-cloud regime. Another regime with high cloud-top clouds (A2) peaks at around 11 km, along with a real middle-level cloud regime (A3) occurring about 11% of the time (which is less frequent than ISCCP C3). This is consistent with previous inferences of a trimodal distribution of tropical convective cloud tops (Johnson et al. 1999). The middle-level cluster occurs in only $\sim$1/3 of the repetitions when daytime-only data are analyzed, replaced instead by a third high cloud cluster with tops at 15 km.

At Nauru, clustering all or daytime only ARSCL data both yield a dominant set of three clusters (Fig. 7 lower panel). A regime of high-top clouds (A1) with peaks at about 13 km occurs about as frequently as the sum of C1 and C2. A second regime with double peaks and low cloud fraction at all levels (A2) occurs about as often as the combination of C3 and C4 at Nauru. A low-cloud regime (A3) occurs roughly as frequently as C5 and C6 combined.

Figure 8 shows the RFO for these ARSCL clusters in each ISCCP cluster and vice versa. At Manus, the highest altitude ARSCL cluster (A1) dominates the disturbed ISCCP states C1 and C2, while the low cloud cluster (A4) is prevalent in the other four ISCCP states, especially the highly suppressed C5. The mid-level ARSCL cluster (A3) does occur often with ISCCP C3 but also with ISCCP C1. Notably, the most highly correlated ISCCP clusters at Manus (C3 and C4) have the most similar associations with

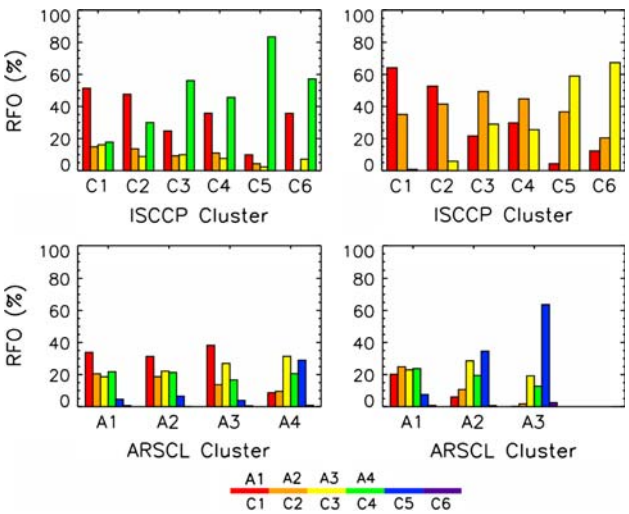

Fig. 8 Relative frequency of occurrence (*RFO*) of ARSCL clusters in each ISCCP cluster (*upper panel*) and vice versa (*lower panel*). The *left column* is for Manus and the *right column* for Nauru. *Upper panel* colors from *red* to *green* represent ARSCL clusters A1–A4. *Lower panel* colors from *red* to *violet* represent ISCCP clusters C1–C6

ARSCL clusters, dominated by A4 and A1 in each case. This reinforces the idea that subtle differences in TAU that affect the ISCCP retrieval of CTP are the primary distinction between C3 and C4. At Nauru (right column), ARSCL clusters A1 and A2 dominate the more disturbed regimes, while the low cloud cluster A3 is most prevalent in the suppressed regimes C5 and C6. Consistently, A3 mostly consists of ISCCP cluster C5. At Nauru as at Manus, C3 and C4 have similar relative occurrences of the ARSCL clusters.

3.4 Tropical cloud regime shifts in the context of MJO

A different perspective on the question of the independence of the ISCCP cloud regimes can be obtained by placing them in a dynamical context. The MJO provides an excellent setting for this. Previous studies document the systematic progression from suppressed conditions dominated by shallow convection and a dry troposphere, through a gradual tropospheric moistening phase, to the outbreak of widespread deep convection, followed by decaying anvil clouds and upper level heating, and a final stabilization during the westerly wind burst period when dry subtropical intrusions once again suppress deep convection (Maloney and Hartmann 1998; Stephens et al. 2004; Kiladis et al. 2005; Tian et al. 2006b; Benedict and Randall 2007). We average ISCCP cluster information into daily (sunlit only) indices at each grid box for a latitude band centered at 1.25°N from 60°E to 180°E. Then we construct a Hovmöller diagram of cluster occurrence in all boreal winter months (November–April) for 2000–2001.

The results are shown in Fig. 9a for the six ISCCP cloud regimes, color-coded from red to violet corresponding to clusters C1–C6. Eastward propagation of the deep convection regime (red) with a period of ~30 days is clearly visible, suggestive of the MJO, with weaker westward propagating components existing at times as well. The sequence at some locations and times suggests a transition from suppressed (blue) to mid-level (yellow) to deep convective and anvil (red, orange) regimes, as envisioned in the discharge–recharge mechanism of tropospheric moisture pre-conditioning of MJO onset (Bladé and

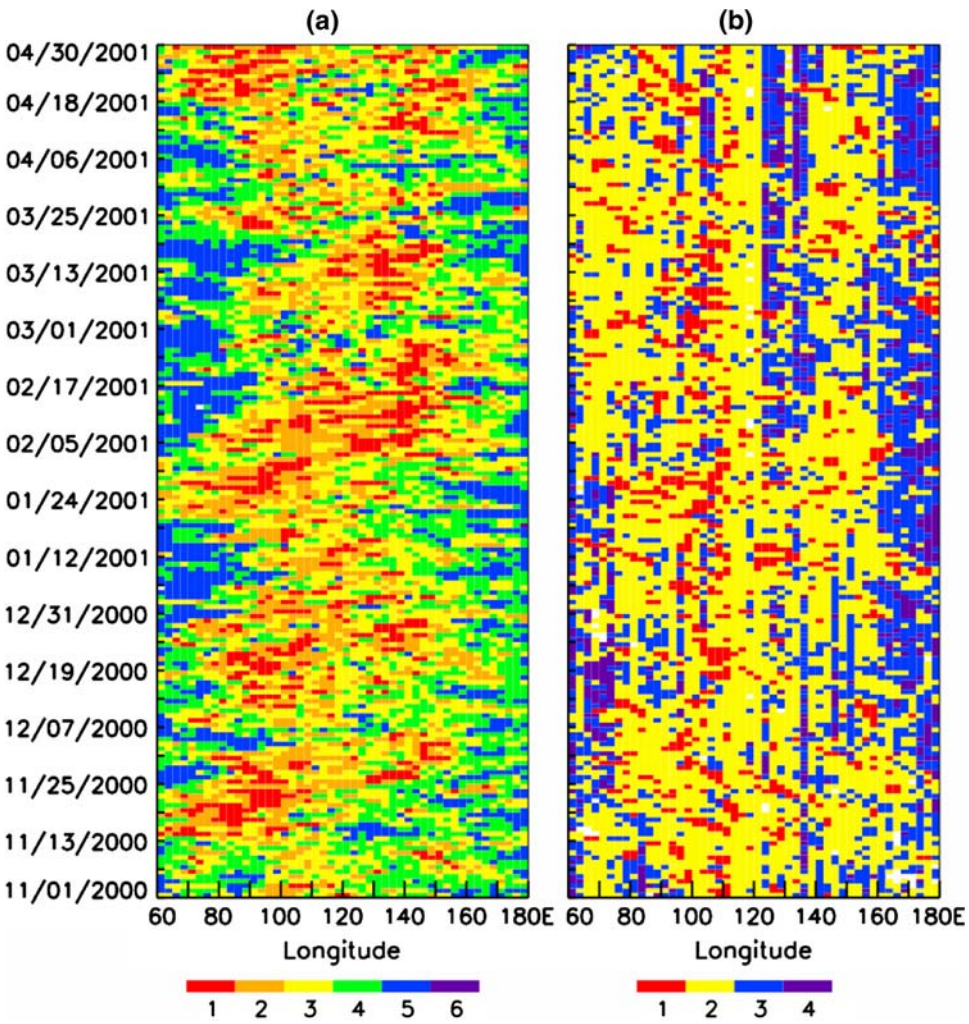

Fig. 9 Hovmöller diagram of daily averaged **a** ISCCP and **b** GCM cloud regime indices from November 2000 to April 2001 in the region 60°E–180°E longitude for the latitude band 0°–2.5°N. Corresponding colors from *red* to *violet* refer to the cloud regimes from C1 to C6 in the *left column*, and from MC1 to MC4 in the *right column*

Hartmann 1993), with anvils and suppressed cloud regimes appearing after deep convection decays. Hovmöller diagrams for other boreal winter months during our study period of 1999–2003 give us similar results (not shown). The timing of the cloud regime propagation is consistent with that of MJO events given in Tian et al. (2006a).

To validate the visual indications from the Hovmöller diagram, we further construct composite RFO bar-charts for each regime using 3-hourly ISCCP cluster indices at seven lag periods in pentads. The regions from 60°E to 180°E within ±5°N are divided into six longitude zones of 20° with center longitudes the same as those used for the MJO index. The peak phase of MJO events is determined near the center longitude of each zone approximately based on negative maxima of the MJO index described in Sect. 2.1.3. Lag 0 refers to a period of ±2.5 days around the peak phase. Negative lag is defined as the longitude zones east of the MJO peak, i.e., preceding it in time. We select the eight strongest out of 11 MJO events detected by Tian et al. (2006a) during 1999–2003 for analysis. The composite only includes longitude bands of each MJO event at which the negative maximum is <-1.

The composite cluster RFOs as a function of MJO phase are presented in Fig. 10. The RFOs of the deep convective (C1, red) and the anvil (C2 orange) regimes increase significantly approaching the peak phase of MJOs, and reach their maxima at the peak phase. After the peak, the occurrence of deep convection decreases immediately while the anvil regime remains for another 5 days or so (lag 1), and decreases gradually afterwards. The mid-level congestus (C3, yellow) and shallow cumulus (C5, blue) regimes dominate several weeks before the MJO peak, decreasing (increasing) before (after) the peak. The shallow cumulus regime decreases more rapidly; by lag −2 the congestus regime is prevalent. The RFO of the cirrus regime (C4, green) is almost constant with MJO phase, suggesting that the presence of isolated cirrus in this tropical region is ubiquitous and not associated with convective activity.

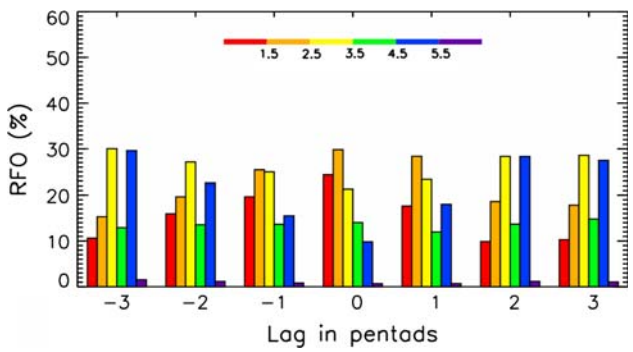

Fig. 10 Relative frequency of occurrence (*RFO*) of each cloud regime at seven lag periods in pentads of eight MJO events in 4 November–April periods from 1999 to 2003. The color scheme for the cloud regimes is the same as in Fig. 9

The coherent progression of the ISCCP regimes is generally consistent with that seen by Benedict and Randall (2007) and suggests that despite the biases discussed in the previous section, the ISCCP histograms do provide independent cloud regime information about six apparently distinct weather states. In particular, the MJO dependence of C3, which is out of phase with C2, versus the MJO-independent behavior of C4 contrasts with the high correlations we find among these regimes when their CTPs are adjusted to match ARSCL. We return to this issue in Sect. 5.

ARSCL provides another source to study the change of cloud structure in the context of MJO. Similar to the way we constructed Fig. 10, we average the available ARSCL vertical cloud profiles during each lag period. Due to missing data in ARSCL, we have to include some weaker MJOs so that we can get as much valid data as possible for all lag periods at Manus. Based on all available ARSCL data we plot the mean vertical cloud profiles in Fig. 11a at each lag. Shape changes in the cloud profiles are clearly seen. A trimodal profile of shallow, mid-level, and cirrus clouds exists 15 days before the peak phase (lag −3). Then from 10 days (lag −2) to 5 days before (lag −1), cloud cover increases and shifts from middle to high levels. At and just after the peak phase, convectively active cloud regimes appear to dominate, with higher tops and greater cloud cover at all levels. Then the cloud cover at all levels rapidly decreases, and the profile has a bimodal distribution of clouds by lag +2. This is the most suppressed MJO phase at Manus; at lag +3, clouds at all levels increase significantly again. The details change depending on how many events are included, and Manus is only a single point with limited data available during MJO periods, but the change in the shape of vertical cloud profile is generally in support of the regime shifts shown in Fig. 10.

Precipitation (Fig. 11b) and relative humidity (RH, Fig. 11c) anomalies at Manus during the MJO phases are in general also consistent with the regime shifts shown in Fig. 10. There is a sharp increase in precipitation at the peak of the MJO, then a more gradual decrease afterwards. RH is anomalously dry in the middle and lower troposphere two pentads before the MJO peak and then increases 5 days before the peak. The moistening spreads upward through the troposphere at the peak and continues to lag 1. At the same time, there is a slight decrease at the lower atmosphere. Finally at lag 2, an abrupt drop in RH appears through most of the troposphere. The drying after the peak phase agrees well with Benedict and Randall (2007), but the pre-conditioning of moisture before the peak only produces mean RH conditions in our anomaly composite.

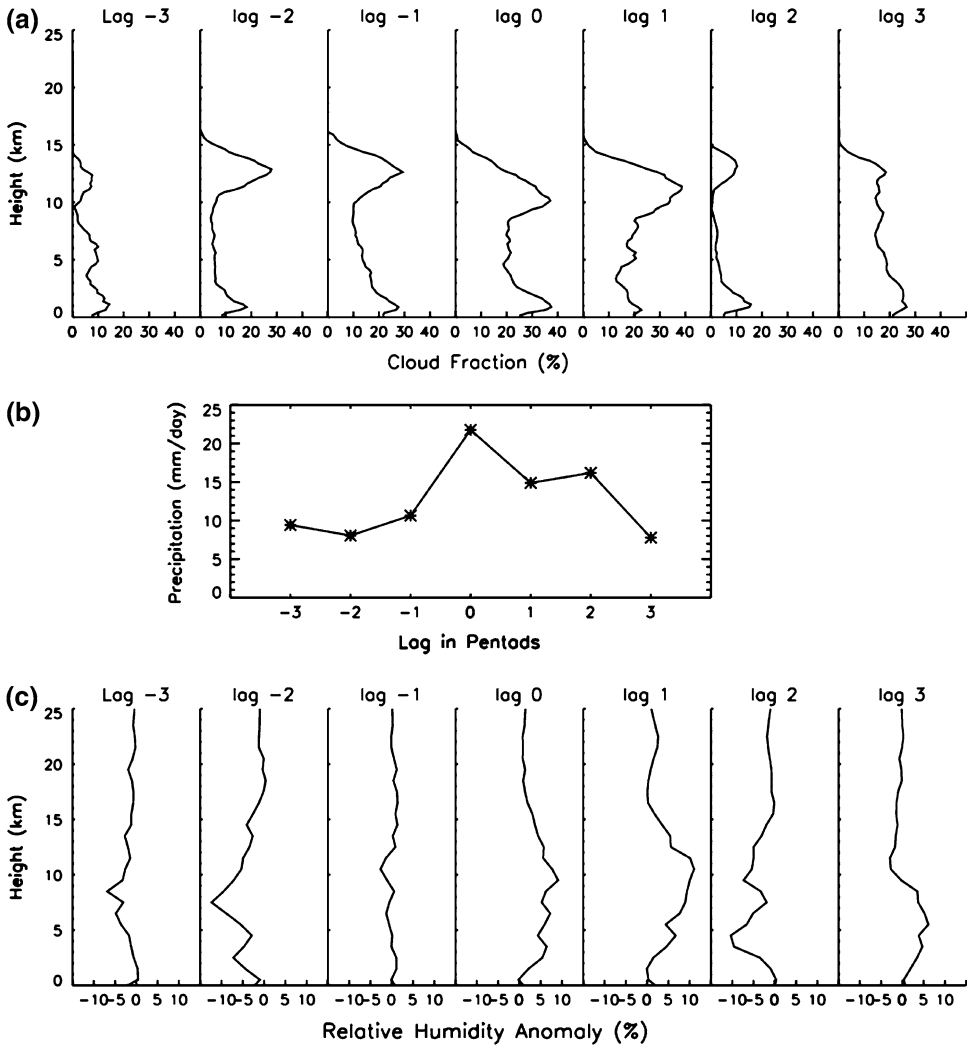

Fig. 11 MJO composites at seven lag periods in pentads at Manus for **a** vertical cloud fraction profiles from ARSCL based on four MJO events; **b** precipitation and **c** relative humidity (*RH*) profiles based on all available MJO events in Fig. 10

4 Cloud regimes in GISS Model E

The results of clustering simulated Model E CTP–TAU histograms are shown in Fig. 12. GCM behavior is less consistent from one run to another, but a set of four independent regimes does emerge in 55% of the runs. Compared to that of ISCCP (Fig. 1), the percentage of cloud at 50–180 mb CTP is underestimated by Model E, while there is too much low-level cloud, especially below the 800 mb level, in all clusters. Euclidean distances between the model and ISCCP regimes are given in Table 2; in general the smallest distance for the disturbed clusters (MC1, MC2) is slightly greater than the inherent ISCCP cluster uncertainty estimated in Table 1, while that for the suppressed clusters is considerably larger. The first regime (MC1) most closely resembles the ISCCP deep convection regime; it occurs most frequently in the ITCZ and SPCZ, as observed (Fig. 13). The second regime (MC2) is a mixture of high optically thin and thick clouds with moderately thick low clouds. Its spatial distribution best matches that of C3, with concentrations in both the ITCZ/SPCZ and tropical land areas, but its CTP–TAU histogram is a better match for the ISCCP suppressed states (Table 2). It is the most common model state, occurring almost half the time. The three cloud types in MC2 occur together in many locations but the optically thick high cloud type is not always present.

The two model suppressed regimes (MC3, MC4) have some similarity to those from ISCCP: an apparent shallow cumulus regime (MC3 vs. C5 in Figs. 1 and 2), and an apparent marine stratocumulus regime (MC4 vs. C6 in Figs. 1 and 2). This resemblance is superficial, however. The RFOs of the suppressed regimes are opposite from those in ISCCP: the observed shallow convection regime is much more frequent than stratocumulus, while their simulated counterparts occur with nearly equal frequency. Furthermore, the scattered cloudiness of ISCCP C5 and more overcast conditions of C6, consistent with their morphological identification, are not reproduced by the model MC3 and MC4 regimes. Further analysis indicates

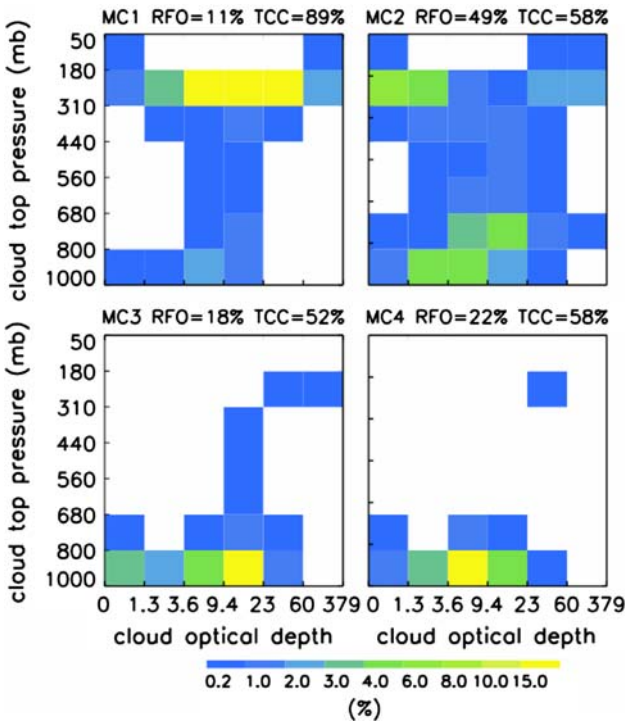

Fig. 12 The mean CTP–TAU histograms of four clusters from 3-hourly GISS Model E ISCCP simulator output over the tropical region of 15°N–15°S. Relative frequency of occurrence (*RFO*) and total cloud cover (*TCC*) are given for each cluster

Table 2 Euclidean distance (%) between the mean CTP–TAU histograms from the GISS GCM and those from ISCCP

GCM	ISCCP					
	C1	C2	C3	C4	C5	C6
MC1	**22.8**	42.4	41.3	56.8	40.1	44.9
MC2	25.4	26.8	17.7	42.3	**10.3**	17.0
MC3	41.7	43.2	36.0	52.8	**31.3**	31.8
MC4	51.0	52.0	45.3	59.8	40.8	**34.2**

The numbers in boldface are the minimum distance for each model cluster

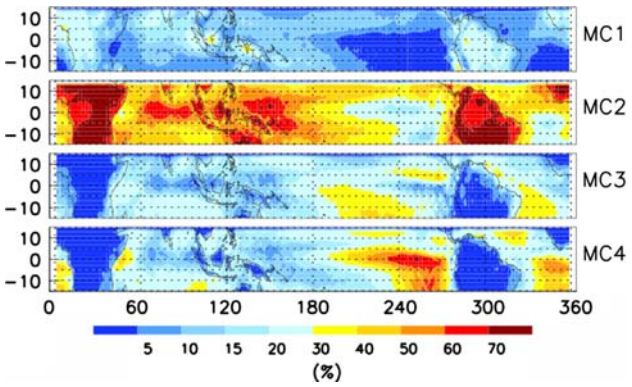

Fig. 13 The corresponding geographic distribution maps of the frequency of occurrence for each cluster in Fig. 12

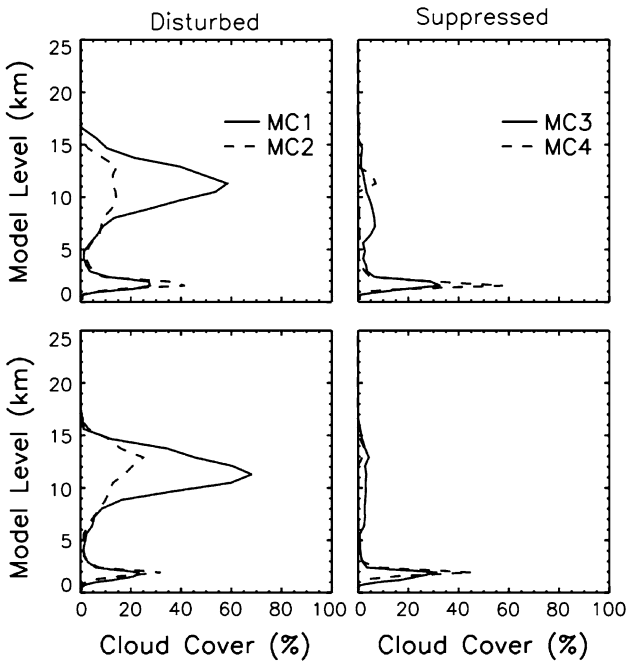

Fig. 14 GCM cloud fraction profiles for each Model E cluster at the Manus (*upper panel*) and Nauru (*lower panel*) gridboxes. The *left panels* represent the disturbed model regimes (MC1, MC2) and the *right panels* the suppressed model states (MC3, MC4)

that in the model there is no real distinction between these two regimes in the physical processes behind them, as we discuss later in this section.

Figure 14 shows the GCM vertical cloud distributions for each regime in the gridboxes that contain Manus and Nauru. Compared to ARSCL, which indicates almost uniform cloud fraction through most of the troposphere in disturbed states, the GCM produces a distinctly bimodal distribution, with little mid-level cloud. Thus, despite the ISCCP mid-level cloud bias, the general impression of deficient GCM mid-level clouds noted in previous studies (Zhang et al. 2005) is in fact the case at least for this model. We also created Hovmöller diagrams analogous to Fig. 9a based on the model's regime classification (Fig. 9b). These show weak anomalies and a preference for westward propagation of the deep convective cloud regime as opposed to the observed dominance of eastward propagating modes in the MJO. This property of the GISS GCM has been previously documented and is a common problem of current GCMs (Lin et al. 2006).

WT07 applied the same clustering method to seven GCMs and found the models to produce a range of 3–7 optimum number of clusters. The GISS GCM differs from all the models analyzed in that paper, for both better and worse. All GCMs in WT07 produce an isolated cirrus regime, but this is absent from GISS Model E. On the other

hand, the shallow cumulus regime is either absent or produces mostly cirrus rather than low cloud in all the WT07 models, while Model E simulates substantial (actually too much) low cloud in this regime. Model E's low cloud optical depths are larger than those in ISCCP, as in the WT07 models, but WT07 note that this is partly an ISCCP bias due to subpixel fractional cloudiness. The "mid-level" regime, which mixes several cloud types, is absent from all models but one in WT07; Model E does produce something like that regime but with less mid-level cloud than observed and more high and low cloud instead.

The names given to the ISCCP regimes are evocative of specific cloud dynamical processes though they are not guaranteed to be causally related to these processes. In the GCM we can easily check how processes contribute to each regime, e.g. by examining the frequency of occurrence of shallow and deep convection and stratiform cloud formation in each of its cloud regimes. We sampled the model simulation at 30 min resolution for one January and July; the resulting RFOs are shown in Fig. 15. As expected, the two suppressed regimes (MC3 and MC4) contain more (less) shallow (deep) convection than the two disturbed convective regimes (MC1 and MC2) do. However, both types of convection occur to some extent in all four model regimes. The two disturbed convective regimes are almost identical to each other, and the two suppressed regimes likewise resemble each other. We also checked the distribution of stratiform low cloud in each regime (not shown). Stratiform low cloud occurs >90% of the time throughout the GCM tropics; the cloud fraction is greatest over the eastern oceans but is generally similar for the MC3 and MC4 regimes. We therefore conclude that in Model E, the association of clusters with specific physical mechanisms is not reliable except for the obvious distinction between deep and shallow processes.

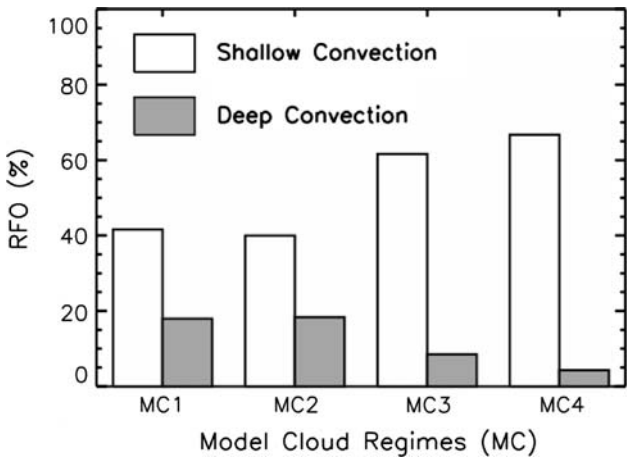

Fig. 15 The relative frequency of occurrence of shallow and deep convection in each Model E cloud regime based on one January and July simulation

Finally, we repeated the clustering analysis with a previous version of the model that does not include the upward transport of convective condensate. This model version produces only three separate regimes, with the two disturbed convective regimes (MC1 and MC2) combined together (not shown). This indicates that pumping condensed water into the upper troposphere helps to better define anvils and convectively generated cirrus as a state distinct from its parent convection, a well-known feature of the lifecycle of convective clusters (Futyan and Del Genio 2007). However this physics does not produce a separate isolated cirrus mode, consistent with our finding (Fig. 10) that the cirrus mode is independent of the convective activity.

5 Summary and conclusions

Tropical cloud regimes defined by cluster analysis of ISCCP CTP–TAU histograms are analyzed in this study to determine their consistency with ARM active remote sensing cloud profiles and their ability to distinguish changes associated with intraseasonal variability. ARSCL cloud-top profiles for each cloud regime indicate that the differences among some of the regimes may not be as prominent as suggested by ISCCP data at least at the ARM TWP sites. Middle level cloud-tops do not dominate any ISCCP cluster at the two ARM TWP sites, though a middle-level cloud regime does occur 11% of the time when we cluster ARSCL profiles. For the deep convection regime ISCCP and ARSCL tend to agree when convection is deepest. Due to the limitations of its algorithm, ISCCP may also wrongly estimate the occurrence of thin clouds in its isolated cirrus regime. Comparisons between times when ARSCL and ISCCP agree versus disagree suggest that errors in the ISCCP histograms are ~5–20% depending on regime. Adjusting the ISCCP histograms to produce CTP profiles that agree with ARSCL eliminates the formal independence of several regimes. This result is a consequence of the almost ubiquitous presence of thin cirrus at high levels in the tropical upper troposphere and small optical thickness variations between clusters that affect passive retrievals of CTP. However, this adjustment is a preliminary estimate because it is applied uniformly to each TAU category. Clustering of ARSCL cloud top height profiles confirms that the ISCCP mid-level congestus and thin cirrus clusters have almost identical cloud vertical distributions, with small TAU differences affecting the accuracy of the ISCCP CTP retrieval to different extents.

At the same time, because ISCCP sometimes sees through thin high clouds and determines a cloud top that is affected by lower level clouds that characteristically differ from one environment to another, it nonetheless provides

some information about six independent cloud regimes despite its ambiguities. This is demonstrated by the presence of systematic changes in the frequency of occurrence of each regime related to the evolution of the MJO. The ISCCP regime evolution is consistent with the discharge–recharge mechanism of the MJO (Bladé and Hartmann 1993): the mid-level congestus regime increases in occurrence relative to the shallow cumulus regime before the peak phase of the MJO and then decreases afterward. Our result is also consistent with the observed pre-conditioning of mid-tropospheric moisture before the MJO peak and drying afterward (e.g. Kiladis et al. 2005; Tian et al. 2006b; Benedict and Randall 2007). But the ISCCP regimes suggest that the idea of a transition from shallow to mid-level to deep convection accounting for MJO onset is in reality more complicated. All ISCCP regimes except stratocumulus exist during all phases. MJO buildup, onset, and decay are more properly described as subtle time changes in the relative occurrence of each state, with the distribution of convective depths shifting gradually from more shallow to more deep before deep convection finally breaks out and dominates.

In summary the ISCCP CTP–TAU histograms are neither what they were intended to be (a distribution of highest cloud top heights) nor what they are sometimes mistaken to be (an actual vertical distribution of clouds), but are instead a hybrid of both. Based strictly on highest top heights at the TWP sites, we conclude that there are really no more than two independent disturbed cloud regimes, differentiated mostly by optical thickness, because high clouds are usually present but not always detected by ISCCP. But based on the Hovmöller diagrams and MJO composites ISCCP does see something that is systematic and dynamically repeatable. This suggests that in a different sense its classification of three disturbed states is useful as an (imperfect) indicator of second cloud layers at lower altitude, where larger differences in cloudiness and cloud properties actually occur. The general correspondence between ISCCP and CloudSat cloud regimes (Zhang et al. 2007) supports this conclusion.

The GISS Model E GCM separates two convective regimes from two suppressed states. The second convectively disturbed regime combines features from several ISCCP regimes. All model regimes contain spurious low clouds, which is consistent with a previous study (Chen et al. 2007). In particular, the model's SPCZ region at times is dominated by low clouds at its eastern end, unlike that observed (Fig. 13). A simulation with a previous version of Model E indicates that vertical convective condensate transport is essential to producing a deep convection regime that is separate from the other high clouds that the convection generates. In this sense the model is doing things in a physically realistic way. However the model-data discrepancies indicate several possible avenues for parameterization improvement. The GCM is deficient in mid-level cloud relative to ARSCL. This suggests the need for higher entrainment rates to make GCM convective cloud tops more sensitive to environmental humidity (see, e.g. Derbyshire et al. 2004). This may also be a factor in the model's inability to simulate MJO-like eastward propagating disturbances. The absence of a GCM isolated cirrus regime and its underprediction of very high cloud tops in its disturbed regimes may point to a cirrus microphysics deficiency. The GCM allows for ice supersaturation but reduces humidity to ice saturation once cirrus form, which may suppress cirrus at later times. Tompkins et al. (2007) suggest a promising approach to this problem.

Model E appears at first glance to be somewhat more successful than other GCMs in simulating the observed suppressed low cloud regimes. However, this is more a limitation of the approach of clustering cloud properties than a true indication of the fidelity of model physics. The model has no actual regime separation between shallow convection and stratiform low cloud, nor does it differentiate the more scattered versus more overcast cloudiness of the two suppressed regimes. This may reflect a more fundamental problem with the simulation of boundary layer clouds, since Model E uses a boundary layer scheme based on dry conserved variables and may have neither sufficient vertical resolution nor a sensitive enough treatment of drizzle, all considered keys to the physics of boundary layer clouds (Wood 2007). On the positive side, the GCM does at least produce frequent shallow convection, which many models do not. The apparent importance of shallow cumulus to cloud feedback (Bony and Dufresne 2005) suggests that optimizing this aspect of the model would be a useful target for enhancing its predictive capability for future climate changes.

Acknowledgments This study was supported by the Cloud Modeling and Analysis Initiative of the NASA Modeling and Analysis Program and by the DOE Atmospheric Radiation Measurement Program. The authors thank Keith Williams, Allyson Sheffield, and George Tselioudis for helpful discussions of cluster analysis. The ISCCP data were obtained from Allyson Sheffield, and the ARSCL data from the ARM archive at Oak Ridge National Laboratory. The k-means clustering algorithm code was downloaded from http://isccp.giss.nasa.gov/tcluster.html. The authors are also thankful for the two anonymous reviewers who provided helpful suggestions that improved the original manuscript.

References

Anderberg MR (1973) Cluster analysis for applications. Academic, New York, p 359

Benedict JJ, Randall DA (2007) Observed characteristics of the MJO relative to maximum rainfall. J Atmos Sci 64:2332–2354

Bladé I, Hartmann DL (1993) Tropical intraseasonal oscillations in a simple nonlinear model. J Atmos Sci 50:2922–2939

Bony S, Dufresne JL, Le Treut H, Morcrette JJ, Senior CA (2004) On dynamic and thermodynamic components of cloud changes. Clim Dyn 22:71–86

Bony S, Dufresne JL (2005) Marine boundary layer clouds at the heart of cloud feedback uncertainties in climate models. Geophys Res Lett 32(20):L20806. doi:10.1029/2005GL0023851

Chang F-L, Li Z (2005) A near-global climatology of single-layer and overlapped clouds and their optical properties retrieved from Terra/MODIS data using a new algorithm. J Clim 18:4752–4771

Chen YH, Del Genio AD, Chen JY (2007) The tropical atmospheric El Niño signal in satellite precipitation data and a global climate model. J Clim 20:3580–3601

Clothiaux E, Ackerman TP, Mace GG, Moran KP, Marchand RT, Miller MA, Martner BE (2000) Objective determination of cloud heights and radar reflectivities using a combination of active remote sensors at the ARM CART sites. J Appl Meteor 39:645–665

Del Genio AD, Wolf AB, Yao M-S (2005) Evaluation of regional cloud feedbacks using single-column models. J Geophys Res 110:D15S13. doi:10.1029/2004JD005011

Del Genio AD, Yao MS, Jonas J (2007) Will moist convection be stronger in a warmer climate? Geophys Res Lett 34:L16703. doi:10.1029/2007GL030525

Derbyshire SH, Beau I, Bechtold P, Grandpeix J-Y, Piriou J-M, Redelsperger J-L, Soares PMM (2004) Sensitivity of moist convection to environmental humidity. Q J R Meteorol Soc 130:3055–3079

Futyan JM, Del Genio AD (2007) Deep convective system evolution over Africa and the tropical Atlantic. J Clim 20:5041–5060

Gordon ND, Norris JR, Weaver CP, Klein SA (2005) Cluster analysis of cloud regimes and characteristic dynamics of midlatitude synoptic systems in observations and a model. J Geophys Res 110:D15S17. doi:10.1029/2004JD005027

Jakob C, Tselioudis G (2003) Objective identi cation of cloud regimes in the Tropical Western Pacific. Geophys Res Lett 30(21):2082

Jakob C, Tselioudis G, Hume T (2005) The radiative, cloud and thermodynamic properties ofthe major Tropical Western Pacific cloud regimes. J Clim 18:1203–1215

Johnson RH, Rickenbach TM, Rutledge SA, Ciesielski PE, Schubert WH (1999) Trimodal characteristics of tropical convection. J Clim 12:2397–2418

Kiladis GN, Straub KH, Haertel PT (2005), Zonal and vertical structure of the Madden–Julian oscillation. J Atmos Sci 62(8):2790–2809

Klein SA, Jakob C (1999) Validation and sensitivities of frontal clouds simulated by the ECMWF model. Mon Weather Rev 127:2514–2531

Lau WKM, Waliser DE (eds) (2005) Intraseasonal variability of the atmosphere-ocean climate system. Springer, Heidelberg, 474 pp

Lin J-L et al (2006) Tropical intraseasonal variability in 14 IPCC AR4 climate models. Part I: convective signals. J Clim 19:2665–2690

Madden RA, Julian PR (1971) Detection of a 40–50 day oscillation in the zonal wind in the tropical Pacific. J Atmos Sci 28(7):702–708

Madden RA, Julian PR (1994) Observations of the 40–50 day tropical oscillation: a review. Mon Weather Rev 112:814–837

Maloney ED, Hartmann DL (1998) Frictional moisture convergence in a composite life cycle of the Madden–Julian Oscillation. J Clim 11:2387–2403

Murphy JM, Sexton DMH, Barnett DN, Jones GS, Webb MJ, Collins M, Stainforth DA (2004) Quantification of modelling uncertainties in a large ensemble of climate change simulations. Nature 430(7001):768–772

Norris JR, Weaver CP (2001) Improved techniques for evaluating GCM cloudiness applied to the NCAR CCM3. J Clim 14:2540–2550

Rayner NA, Parker DE, Horton EB, Folland CK, Alexander LV, Rowell DP, Kent EC, Kaplan A (2003) Global analyses of SST, sea ice and night marine air temperature since the late nineteenth century. J Geophys Res 108:4407. doi:10.1029/2002JD002670

Rossow WB, Schiffer RA (1999) Advances in understanding clouds from ISCCP. Bull Am Meteorol Soc 80:2261–2288

Rossow WB, Tselioudis G, Polak A, Jakob C (2005) Tropical climate described as a distribution of weather states indicated by distinct mesoscale cloud property mixtures. Geophys Res Lett 32:L21812. doi:10.1029/2005GL024584

Schmidt GA et al (2006) Present day atmospheric simulations using GISS Model E: comparison to in-situ, satellite and reanalysis data. J Clim 19:153–192

Stephens GL, Webster PJ, Johnson RH, Engelen R, L'Ecuyer T (2004) Observational evidence for the mutual regulation of the tropical hydrological cycle and tropical sea surface temperatures. J Clim 17:2213–2224

Tian BJ, Waliser DE, Fetzer EJ (2006a) Modulation of the diurnal cycle of tropical deep convective clouds by the MJO. Geophys Res Lett 33:L20704. doi:10.1029/2006GL027752

Tian BJ, Waliser DE, Fetzer EJ, Lambrigtsen BH, Yung YL, Wang B (2006b) Vertical moist thermodynamic structure and spatial-temporal evolution of the MJO in AIRS observations. J Atmos Sci 63(10):2462–2485

Tompkins AM, Gierens K, Rädel G (2007) Ice supersaturation in the ECMWF integrated forecast system. Q J R Meteorol Soc 133:53–63

Wang J, Rossow WB, Uttal T, Rozendaal M (1999) Variability of cloud vertical structure during ATEX observed from a combination of rawinsonde, radar, ceilometer, and satellite. Mon Weather Rev 127:2484–2502

Webb M, Senior C, Bony S, Morcrette JJ (2001) Combining ERBE and ISCCP data to assess clouds in the Hadley Centre, ECMWF and LMD atmospheric climate models. Clim Dyn 17:905–922

Williams KD, Tselioudis G (2007) GCM intercomparison of global cloud regimes: present-day evaluation and climate change response. Clim Dyn 29:231–250

Williams KD, Senior CA, Slingo A, Mitchell JFB (2005) Towards evaluating cloud response to climate change using clustering technique identification of cloud regimes. Clim Dyn 24:701–719

Wood R (2007) Cancellation of aerosol indirect effects in marine stratocumulus through cloud thinning. J Atmos Sci 64:2657–2669

Zhang CD (2005), Madden–Julian oscillation. Rev Geophys 43(2):RG2003. doi:10.1029/2004RG000158

Zhang MH, Lin WY, Klein SA, Bacmeister JT, Bony S, Cederwall RT, Del Genio AD, Hack JJ, Loeb NG, Lohmann U, Minnis P, Musat I, Pincus R, Stier P, Suarez MJ, Webb MJ, Wu JB, Xie SC, Yao M-S, Zhang JH (2005) Comparing clouds and their seasonal variations in 10 atmospheric general circulation models with satellite measurements. J Geophys Res 110:D15S02. doi:10.1029/2004JD0005021

Zhang Y, Klein S, Mace GG, Boyle J (2007) Cluster analysis of tropical clouds using CloudSat data. Geophys Res Lett 34:L12813. doi:10.1029/2007GL029336